*Desalination and Water Treatment*
www.deswater.com

51 (2013) 2231–2243
February


doi: 10.1080/19443994.2012.734729

Taylor & Francis
Taylor & Francis Group

# Numerical simulation of flashing process in MSF flash chamber

M. Khamis Mansour*[,1], Hassan E.S. Fath

*Faculty of Engineering, Mechanical Department Alexandria University, Alexandria, Egypt*
*Fax: +20 3597 1853; email: m.mansour@bau.edu.lb*

Received 19 December 2011; Accepted 5 August 2012

ABSTRACT

Multistage flash (MSF) technology is widely used in saline water desalination particularly in Middle East and North Africa and Gulf Cooperation Council countries. Enhancement in the thermal performance of this technology in different plant sections and processes including the brine flashing process is still promising. This study addresses the optimal position of jumping plate (weir) location and its number inside the MSF chamber. The optimization exercise has been carried out in terms of maximum flashing vapor production and lower pressure drop using commercial computational fluid dynamics software ANSYS CFX 12.1. The Eulerian–Eulerian (free surface flow) two-phase model was adopted while a $k$–$\varepsilon$ model was used a turbulent flow model. The theoretical model was verified by comparing the predicated results with those obtained from the reference case study. The maximum deviation between both results was found to be within 8.3%. Prediction of velocity vectors, phase volume fraction, and temperature profile are presented. The results showed that a middle single weir in the flash chamber has the highest thermal and hydraulic performance.

*Keywords:* Desalination; MSF; Flashing; Evaporation; Two-phase flow; CFD

## 1. Introduction

In the multistage flash (MSF) process, vapor forms within the liquid bulk via flashing process and hot brine flows freely in series of successive flash chambers (FCs), where flashing occurs because of the successive reduction of the stages pressure below the brine temperature. Flashing process is one of the main features of the MSF in which scale formation on the surface of the tubes is eliminated. The flashed-off vapor condenses on the tubes of the preheater/condenser units. Fig. 1 shows the overall configuration of a typical of an operating MSF chamber and its main components. Flashed brine in the form of vapor passes through demister and condenses on the condenser tubes. Distilled water is accumulated in a distillate tray and transferred to the next stage as shown in Fig. 1.

Thermodynamically, flashing occurs in the MSF chamber when the flowing brine is exposed to a sudden pressure drop below the equilibrium vapor pressure corresponding to the brine temperature. Under adiabatic operating conditions, part of the liquid vaporizes to regain equilibrium and draws its latent heat of vaporization from the remaining brine bulk. The brine temperature drops towards the equilibrium temperature corresponding to the lower pressure. The flashing process in MSF plants is usually considered to be in thermodynamic equilibrium. There are, however, considerable differences between thermodynamic equilibrium and the actual processes when flashing develops continuously. Brine needs more time to reach the thermodynamic equilibrium than

*Corresponding author.

[1]Present address: Mechanical Department, Faculty of Engineering, Beirut Arab University, Riad El Solh 1150 20, Beirut, Lebanon. Tel. +961 71817351; Fax: +961 7 985060.

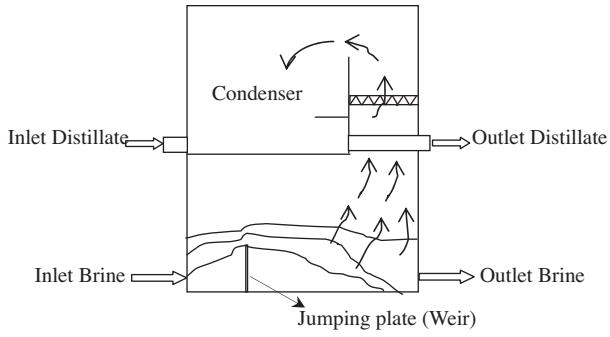


Fig. 1. MSF flash chamber.

what takes place in the MSF FC. Therefore, the brine coming out of the FC always retains some residual superheat which considerably influences both the technical and economical characteristics of the MSF plant design; the smaller is the residual superheat, the higher is the thermal performance of flashing process and the MSF plant.

Flashing in a MSF distillation plant takes place in two ways. Firstly, it occurs by free evaporation at the free surface of the brine and secondly, in the form of bubbles forming within the bulk of the brine. The evaporation due to both free surface evaporation and ebullition is integrally linked with the thermofluid processes of fluid dynamics, heat transfer, mass transfer, and thermodynamics. The complexity of the flashing process still hinders detailed modeling and innovative improvements of the process. Even the correlations developed for characterizing the process provide results that vary widely from each other, depending upon many factors including the flashing technique, Fath [1]. Understanding the flashing process in the MSF distillation plant is essential, therefore, for any comprehensive attempt to improve the flashing process and to enhance both heat and mass transfer rates. The problem is difficult to solve, either theoretically or experimentally. This fact is evidenced by the relatively small amount of published data, as well as by the number of conflicting conclusions.

As aforementioned, according to authors' knowledge, the open studies available in literature on the numerical evaporation flashing are very rare and insufficient. Fath [1] concluded that through a theoretical study for flashing process of selected pilot test unit, the thermodynamic nonequilibrium factor can be reduced by increasing the brine superheat, flashing surface area, number of active nucleation sites, and brine residence time inside the FC. Lee and Seul [2] investigated the effect of brine liquid level on the flow behaviors on the evaporation performance of the MSF unit. The authors solved a steady-state, turbulent flow, and two-dimension governing equations for the liquid phase along with the bubble motion equations using the PSI-Cell method. The authors showed that the evaporation performance is improved with lower liquid level inside the FC. El-Dessouky et al. [3] developed a number of design correlations of the MSF flashing stage including discharge coefficient, nonequilibrium factor, and overall heat transfer coefficient based on a large database obtained experimentally for six large-scale MSF units located in different stations in the Gulf States during steady-state operation. The correlations for the discharge coefficient and the nonequilibrium factor were developed for two different types of interstage devices. Also, the overall heat transfer coefficient correlation was obtained for both the heat recovery and heat rejection sections. Jin and Low [4] conducted an experimental work using a transparent flash evaporation chamber to simulate the single-phase seawater flow in the flash stage in the MSF desalination process. They measured field fluid flow velocity vectors in the chamber using a particle image velocimetry system to study the effects of main flow parameters such as water level and flow rate on flow patterns. The fluid flow in the chamber was also numerically simulated using a two-dimensional $k$–$\varepsilon$ turbulent flow model. The simulated results were compared with the test data. The results show that a large recirculation region with several vortices embedded would be generated at a higher water level or at a larger flow rate.

This article investigates numerically the flashing process in typical MSF operating plant focusing on the effect of the weir (jumping plate) location and its number on the thermal and hydraulic performance of the flashing process.

## 2. Mathematical modeling

Multiphase flow refers to the situation where more than one fluid is present. Each fluid may possess its own flow field, or all fluids may share a common flow field. Unlike multicomponent flow, the fluids are not mixed on a microscopic scale in multiphase flow. Rather, they are mixed on a macroscopic scale, with a discernible interface between the fluids. ANSYS CFX includes a variety of multiphase models to allow the simulation of multiple fluid streams, bubbles, droplets, solid particles, and free surface flows which is suitable for the flash evaporation. Two distinct multiphase flow models are available in ANSYS CFX, Eulerian–Eulerian multiphase model and a Lagrangian particle tracking multiphase model. Eulerian–Eulerian multiphase model has been adopted in this study. The effects of the salt particles and condensable gases are not considered in this study for simplicity purposes.

Therefore, the multiphase model involves two components only (water liquid and water vapor). The following section presents the derivation of the governing equations that are solved by ANSYS CFX.

### 2.1. Conservation of mass

The description of multiphase flow as interpenetrating continua incorporates the concept of phasic volume fractions, denoted here by $\alpha_{q.}$ Volume fractions represent the space occupied by each phase, and the laws of conservation of mass and momentum are satisfied by each phase individually.

The tracking of the interface(s) between the phases is accomplished by the solution of a continuity equation [5] for the volume fraction of one (or more) of the phases. For the $q$th phase, this equation has the following form:

$$\frac{1}{\rho_q}\left[\frac{\partial}{\partial t}(\alpha_q\rho_q) + \nabla\cdot\left(\alpha_q\rho_q\vec{v}_q\right) = \sum_{p=1}^{n}\left(\dot{m}_{pq} - \dot{m}_{qp}\right)\right] \quad (1)$$

where $\rho_q$ and $\vec{v}_q$ are the density and velocity of phase $q$, respectively. $\dot{m}_{qp}$ characterizes the mass transfer from phase $q$ to phase $p$ and $\dot{m}_{qp}$ is the mass transfer from phase $p$ to phase $q$. $n$ is the number of components for the multiphase flow which is two in this study.

The volume conservation equation is:

$$\sum_{q=1}^{n}\alpha_q = 1 \quad (2)$$

### 2.2. Conservation of momentum

The momentum balance for phase $q$ yields

$$\frac{\partial}{\partial t}\left(\alpha_q\rho_q\vec{v}_q\right) + \nabla.\left(\alpha_q\rho_q\vec{v}_q\vec{v}_q\right) = -\alpha_q\nabla p + \nabla\cdot\left(\tau_m + \tau_{tm} + \tau_{dm}\right) + \alpha_q p_q\vec{g} \quad (3)$$

### 2.3. Conservation of energy

The energy equation, also shared among the phases, is shown below.

$$\frac{\partial}{\partial t}(\rho E) + \nabla\cdot(\vec{v}(\rho E + p)) = \nabla\cdot(k_{eff}\nabla T) \quad (4)$$

The energy $E$ and temperature $T$ are treated as mass-averaged variables:

$$E = \frac{\sum_{q=1}^{n}\alpha_q\rho_q E_q}{\sum_{q=1}^{n}\alpha_q\rho_q}$$

where $E_q$ for each phase is based on the specific heat of that phase and the shared temperature. The properties $\rho$ and $k_{eff}$ (effective thermal conductivity) are shared by the phases.

### 2.4. Model assumptions and boundary conditions

The following assumptions are postulated in the CFD model: (a) two dimensions flow, (b) steady-state, (c) Newtonian flow, (d) incompressible flow, (e) Turbulent flow using $k-\varepsilon$ model. At the inlet section, the velocity and temperature of the brine are considered as uniform along the gate entrance while at the outlet section, opening type of boundary condition with unspecified outlet temperature and pressure for the steam and water, respectively. The entire domain wall is considered adiabatic with no slip condition.

### 2.5. Reference case study

The FC unit of Sidi Krir MSF (Alexandria–Egypt) [6] has been selected as the case study in this work. Sidi Krir MSF plant consists of 20 stages with a production capacity of 5,000 $m^3$/day of desalinated water with brine recirculation flow rate of 1847 t/h. The plant first FC operating conditions are taken as the base case study; Fig. 2 shows more details of the internal of Sidei Krir plant and its FC internal configuration. The typical first-stage design conditions are: (a) the brine inlet temperature is 110°C; (b) the brine exit temperature is 106°C; (c) the brine mass flow rate is 1847 t/h; (d) the stage pressure is 1.023 bars; (e) the flashed vapor is 12.5 ton/h for the full domain; and (f) the steam saturation temperature is 102°C.

### 2.6. Mesh generation and numerical approach

Vapor–brine flow domain inside Sidi Krir FC and the FC dimensions are given in Fig. 3. The grid description for the FC with a jumping plate located in the middle length of the FC is presented in Fig. 4. Two meshes were generated for the calculations and the grid independence test. The coarse grid consisted of 32,987 cells with a maximum volume of $2.5\times10^{-5}$ and the fine grid consists of 197,568 cells with a maximum volume of $6.25\times10^{-6}$. The grids were generated


Fig. 2. Sidi Krir MSF plant and FC [6].

by meshing all faces using regular quadrilateral mesh elements and meshing the volume as shown in Fig. 3. As the flow was wall dominated, the mesh is extended into the viscous sublayer such that $y+ \leq 5$ in the wall bounded mesh points and so that enhanced wall functions could be used with $k-\varepsilon$ model. Both region-adaptive refinement and boundary-adaptive refinement were used in mesh adaptation facilities in ANSYS CFX in the calculation with the coarse grid in order to get a reasonable solution. The volume of fluid method [7] was used to allow the free-surface to deform freely with the underlying turbulence. A second-order upwind scheme was applied for space discretization of the governing equations. The PISO algorithm [8] and PRESTO! scheme [9] was adopted for the velocity–pressure coupling and pressure interpolation, respectively. The turbulent stresses in the mixture momentum Eq. (3) can be modeled by any of the standard turbulence closures. $k-\varepsilon$ model [10] was chosen as a turbulent model owing to its robustness and it has low computational time compared with the other turbulence model. However, $k$–$\omega$ [11],12] was also tried as a turbulent model in a single run of the numerical analysis and the difference between the two models ($k$–$\varepsilon$) and ($k$–$\omega$) was insignificant (less than 1%). The fluid buoyancy model was treated using Boussinesq approach. The simulation was performed on Pentium processor T3400 with 2 GB RAM. The solution attains its convergence after several hundreds of iterations with residuals of $10^{-4}$ for the continuity, volume fraction, turbulence parameters, and momentum equations and $10^{-6}$ for the energy equation. The computational time for a single iteration required approximately 3–5 min.

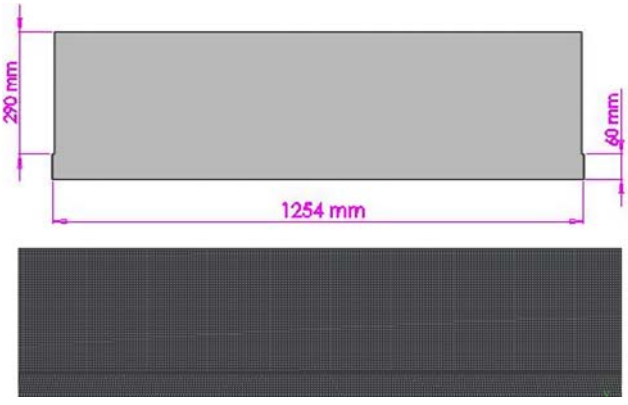


Fig. 3. Sidi Krir FC dimension and mesh size.

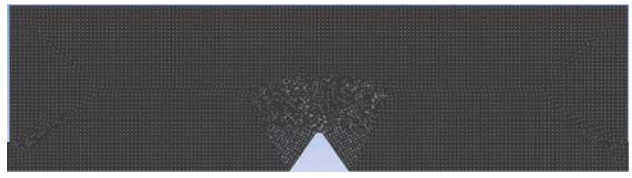

Fig. 4. Grid configuration of FC with middle jumping plate.

## 3. Results and discussion

### 3.1. Simulation of the flashing process for the reference case study

The numerical results shown in Fig. 5(a)–(d) represent the theoretical thermofluid performance of the reference case (without jumping plate). The calculated mass flow rate of the flashed vapor is 11 kg/s while the actual vapor mass flow rate for the reference case study is 12 kg/s; i.e. the deviation between the theoretical analysis and the reference case is 8.3% which is reasonable. The thermofluid performance of the FC is represented by the distribution of volume vapor fraction, brine temperature, and brine velocity along the FC length as illustrated in Fig. 5(a)–(d). As Fig. 5(b) shows, the brine enters at a higher temperature of 110°C then the brine temperature is cooled downward the flow path until it exits at temperature of 106.4°C. It is interesting to see that despite the higher temperature distribution occurred at the first half of the FC

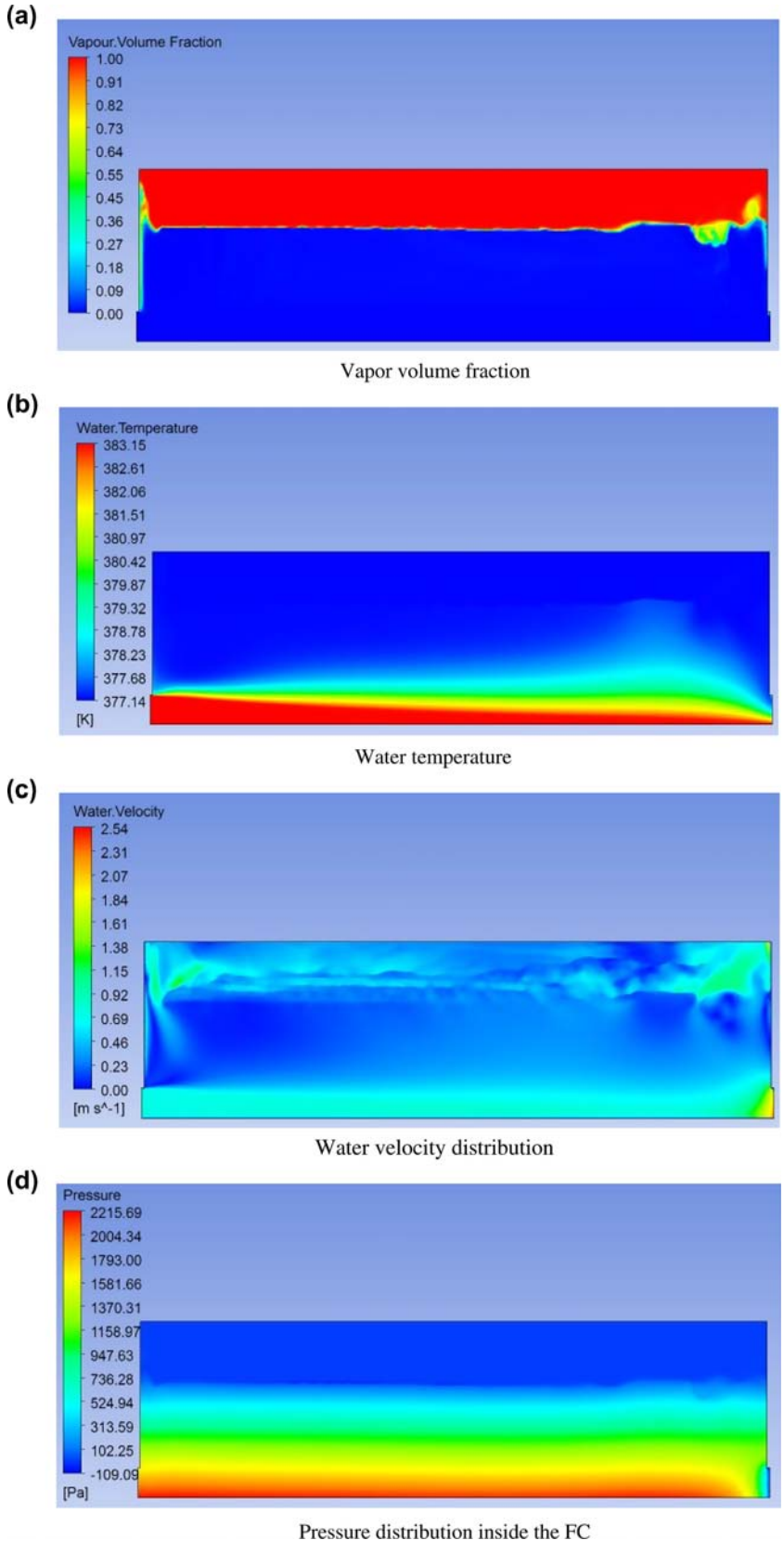


Fig. 5. Thermofluid performance along the FC length (no weir).

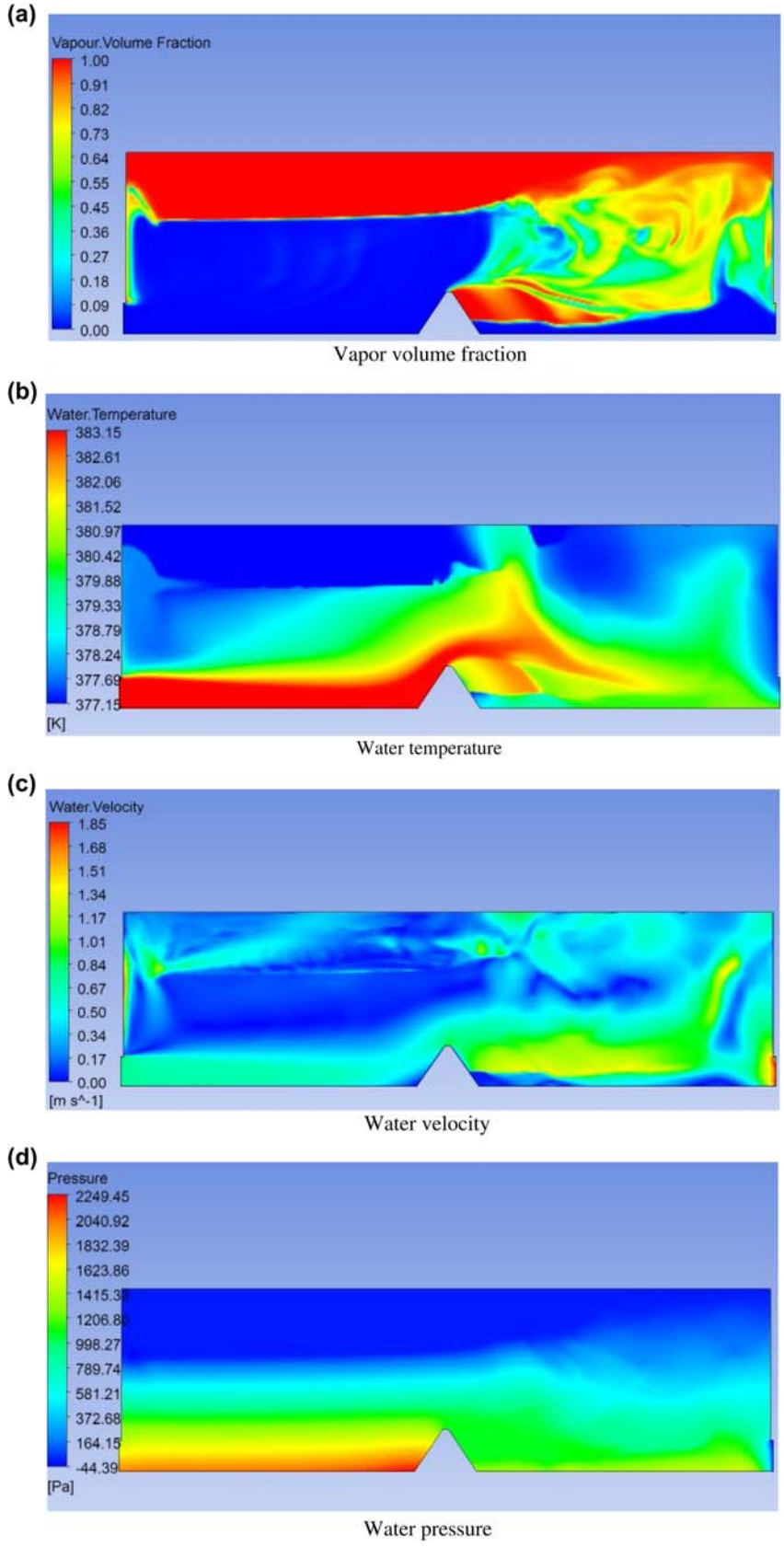


Fig. 6. Thermofluid performance along the FC length (single-middle weir).

length, the volume vapor fraction is smaller at the entrance gate of the brine as shown in Fig. 5(a). This could be explained by Fig. 5(c), due to the enlargement/expansion effect of the water flow inside the chamber; and the brine velocity is increased significantly from 1.03 to 3.55 m/s at the FC left wall near the entrance gate. The higher velocity vectors stimulate the water droplets to rise up in the direction increasing the carryover factor in the zone as shown in Fig. 5(a). It should also be observed from Fig. 5(a) that the thickness of the flashing process represented by the volume vapor fraction is larger at some distance close to the entrance gate which gets slimmer afterwards. The explanation is that the flashing heat transfer rate is proportional to the cubic difference between the brine temperature and saturation temperature, Fath [1]. Hence, at the beginning, this difference is extremely high then the brine temperature is gradually dropped. The more temperature difference the more flashing evaporation is produced. Fig. 5(d) displays the pressure distribution along the FC length. As observed from this figure, the pressure gradient in the transverse direction of the FC indicates to the expansion effect of the flashing process.

### 3.2. Effect of using single jumping plates (weir) on the flashing process

Fig. 6(a)–(d) shows the effect of using a single weir (jumping plate) on the thermal and hydraulic performance of the flashing process. The jumping plate is located at the FC center and assumed of triangle configuration of height equal to 1.25 times the entrance gate opening. As abovementioned, the flashing process depends principally on both the free evaporation at the free surface of the liquid and on the flashing ebullition of bubbles formulation within the bulk of the liquid. The main aims of using the jumping plate are to: (a) act as turbulence generator and (b) activate the nucleation sites for bubbles formation in order to improve the flashing and surface evaporation processes in terms of increasing vapor production.

As shown in Table 1, the flashed vapor mass flow rate has been increased from 11 t/h in the reference case (with no plates) to 13 t/h with single jumping plate. This is evidenced by the value of the outlet water temperature which has been reduced, i.e. the nonequilibrium factor has been reduced as a result of the enhancement in the heat and mass transfer coefficients. The outlet temperature in the first case is 379.4˚K (106.4˚C) while in the second case it is of 378.7˚K (105.7˚C). On the other hand, the hydraulic pressure drop has increased in the second case by 0.08 kPa and the amount of vapor volume fraction exiting from the exit water gate has increased from 0.053 to 0.203 as well. Therefore, it may be concluded that the usage of a jumping plate will enhance the thermal performance coupling with deterioration in the flashing hydraulic performance to some extent. However, the enhancement in the thermal performance which is interpreted by the increase in vapor mass flow rate dominates the drop in the hydraulic performance, i.e. the increase in vapor flow rate is 18.2% while the increase in flow pressure drop is only 4.8%. It should be noted that the more increase in stage pressure drop is translated to a negative effect on the following flashing stage performance. The designer should consider both the hydraulic and thermal performance of the flashing process. But what is optimum number of jumping plates to be used or what is the significant effect of using multiple jumping plates on the thermal and hydraulic performance of the flashing process. This will be discussed in details in the following section.

### 3.3. Effect of using multiple jumping plates on the flashing process

The effect of using two and three jumping plates is studied and the results are presented in Figs. 7 and 8. It might be expected that the increase in number of plates "tabulators" will account to an enhancement in the thermal performance in the flashing process. However, contrary to this perception, an increase in the number of jumping plates could harm the thermal performance of the flashing process.

Table 1
Comparison of performance characteristics between two different cases

| Case | Vapor flow rate (t/h) | Water outlet temperature (˚K) | Average vapor volume fraction at steam outlet | Average vapor volume fraction at water outlet | Calculated pressure drop (kPa) |
|---|---|---|---|---|---|
| Without jumping plate | 11 | 379.4 | 1 | 0.053 | 1.65 |
| With jumping plate | 13 | 378.7 | 0.995 | 0.203 | 1.73 |

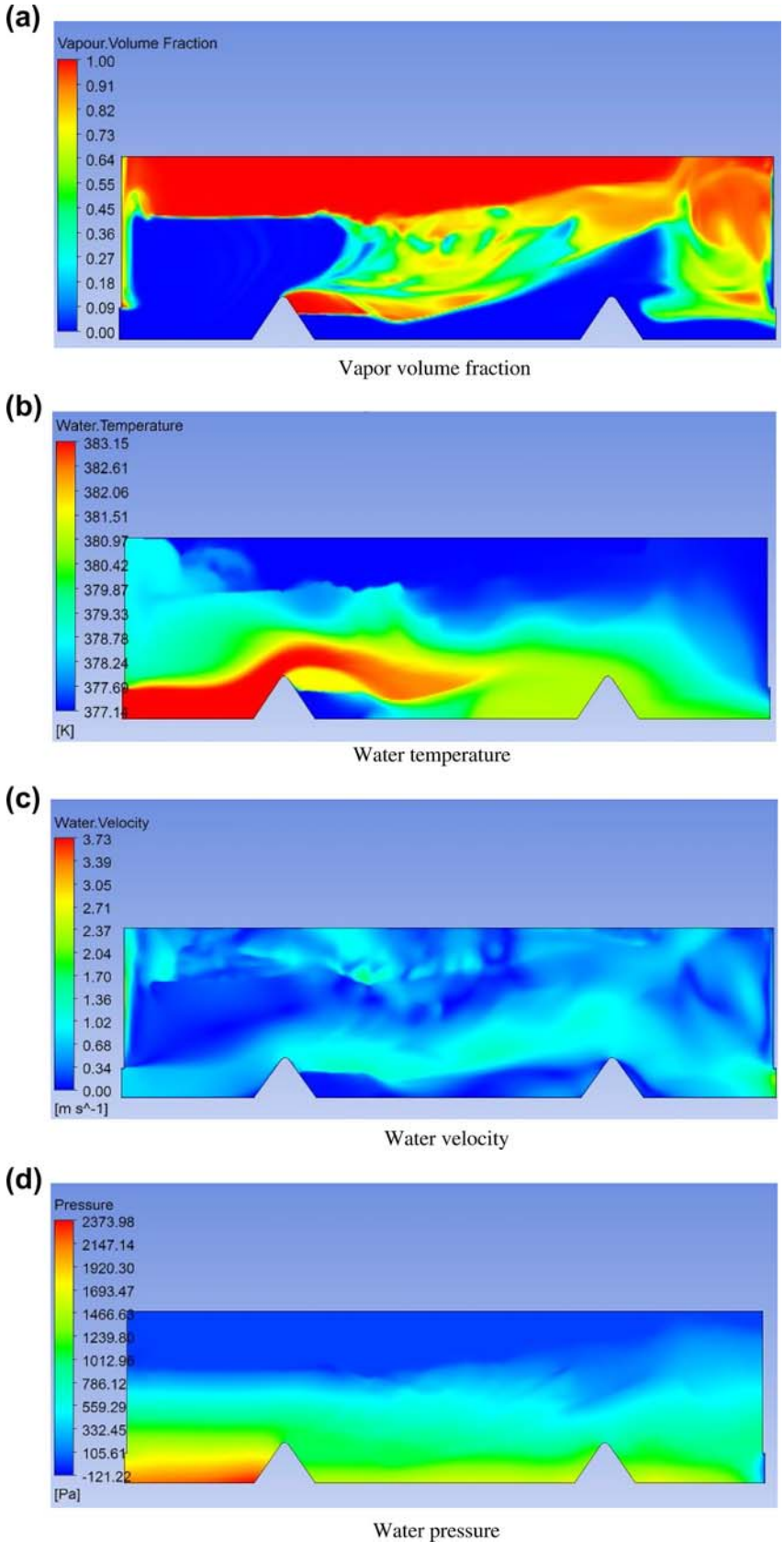


Fig. 7. Thermofluid performance along the FC length (two weirs).

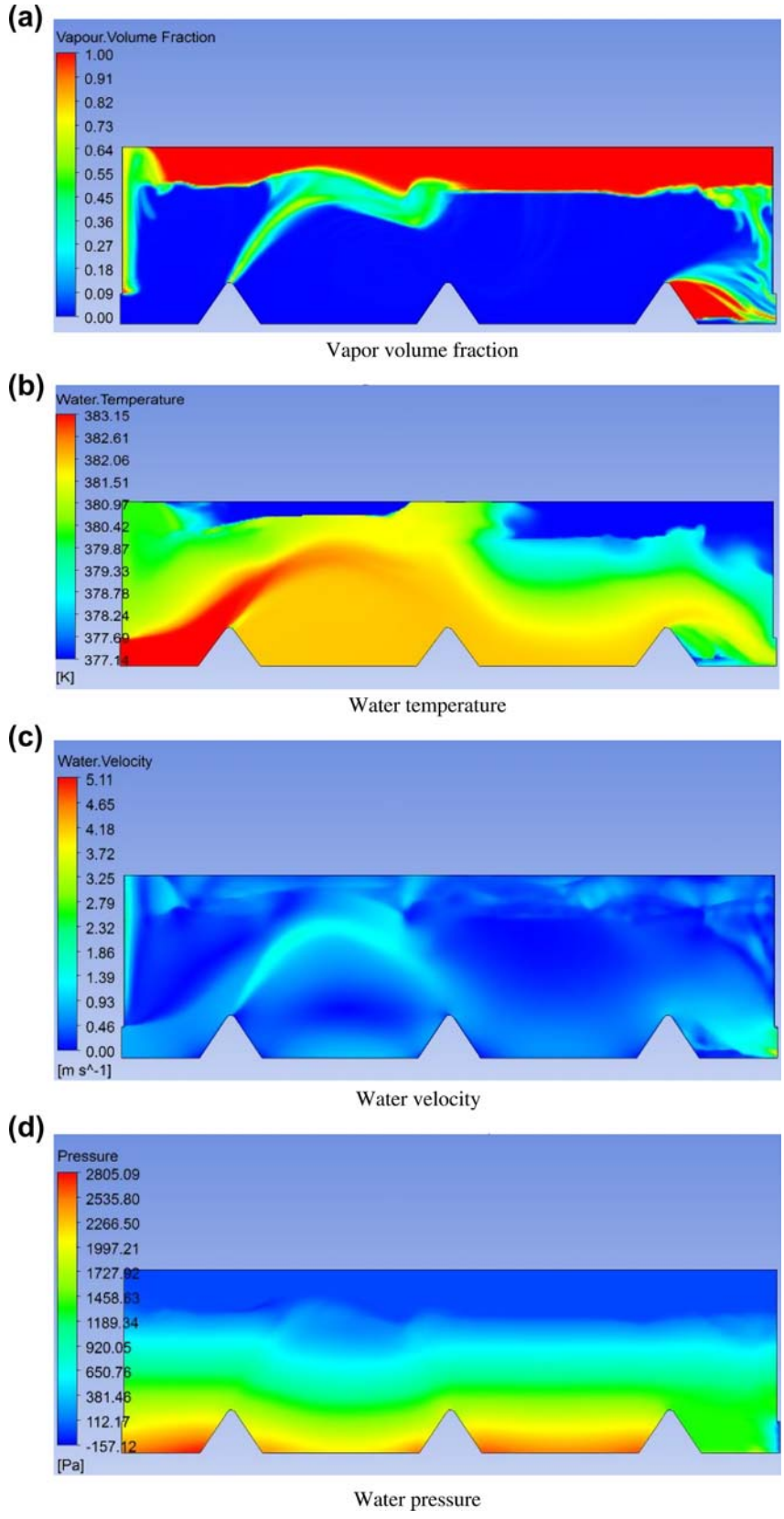


Fig. 8. Thermofluid performance along the FC length (three weirs).

Table 2
Comparison of performance characteristics between four different cases

| Case | Vapor flow rate (t/h) | Water outlet temperature (°K) | Average vapor volume fraction at steam outlet | Average vapor volume fraction at water outlet | Calculated pressure drop (kPa) |
|---|---|---|---|---|---|
| Without jumping plate | 11 | 379.4 | 1 | 0.053 | 1.65 |
| With single jumping plate | 13 | 378.7 | 0.995 | 0.203 | 1.73 |
| With two jumping plate | 12.82 | 378.8 | 0.984 | 0.225 | 1.85 |
| With three jumping plate | 8.54 | 380.2 | 0.989 | 0.398 | 2.25 |

Table 3
Comparison of the performance characteristics between the three different locations

| Case | Vapor flow rate (t/h) | Water outlet temperature (°K) | Average vapor volume fraction at steam outlet | Average vapor volume fraction at water outlet | Calculated pressure drop (kPa) |
|---|---|---|---|---|---|
| Middle location | 13 | 378.7 | 0.995 | 0.203 | 1.73 |
| One-third location | 9.05 | 380 | 0.993 | 0.074 | 1.81 |
| Two-third location | 8.54 | 380.2 | 1 | 0.25 | 1.52 |

Table 2 shows that the vapor flow rate has been slightly reduced with two jumping plates when compared with a single plate from 13 to 12.82 t/h with two jumping plates and drops to 8.54 t/h (34.3%) with three jumping plates. The value of the outlet water temperature is considered as an indicator for the thermal performance trend. Meanwhile, the pressure drop consistently increases with increasing number of plates as shown in Table 2. It may be concluded that using of a single plate is considered the best solution in this study. On the other hand, using three jumping plates constitutes the worst condition of the three cases of Table 2. Although the increase in number of plates results in an enhancement in the turbulence augmentation at expense of the increase of the static pressure drop, however, this case has the lowest value of the steam flow rate of 8.54 kg/s. The reason is attributed to the location of the three plates along the channel length, which decreases the heat transfer surface area for the liquid–vapor interface compared with the two previous cases (see Figs. 6(a), 7(a), and 8(a). This reduction in the liquid–vapor surface area outweighs the enhancement in the liquid–vapor heat transfer coefficient. Accordingly, this case is characterized by low thermal performance comparing with those of the other cases.

### 3.4. Optimum location of the single jumping plate (weir)

Three positions of the single jumping plate are studied to define the optimum location of the jumping plate; the first position is at the first one-third of the FC length, the second position is at the middle, and the third position is at the two-third point of the FC length. The results show that the middle position represents the optimal location for the jumping plate. The comparison of the performance characteristics between the three locations is given in Table 3 and the numerical results are exhibited in Figs. 9 and 10 in addition to Fig. 6.

As Table 3 indicates, the middle position of a single plate achieves the highest steam production while the one-third position attains the lowest dryness fraction exiting with the water to the following stage. Alternatively, the two-third location has the lowest

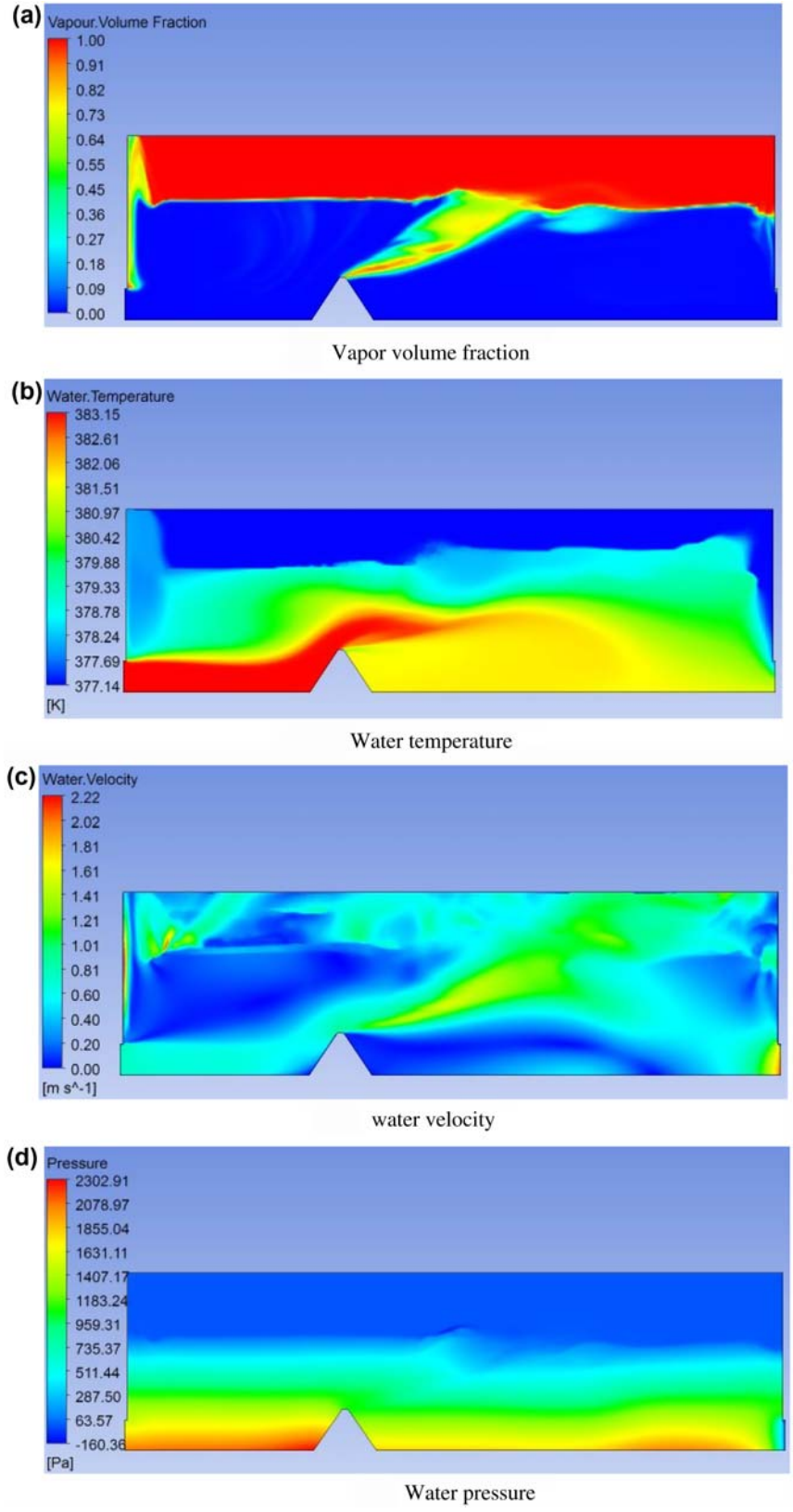


Fig. 9. Thermofluid performance along the flash chamber length (one third location).

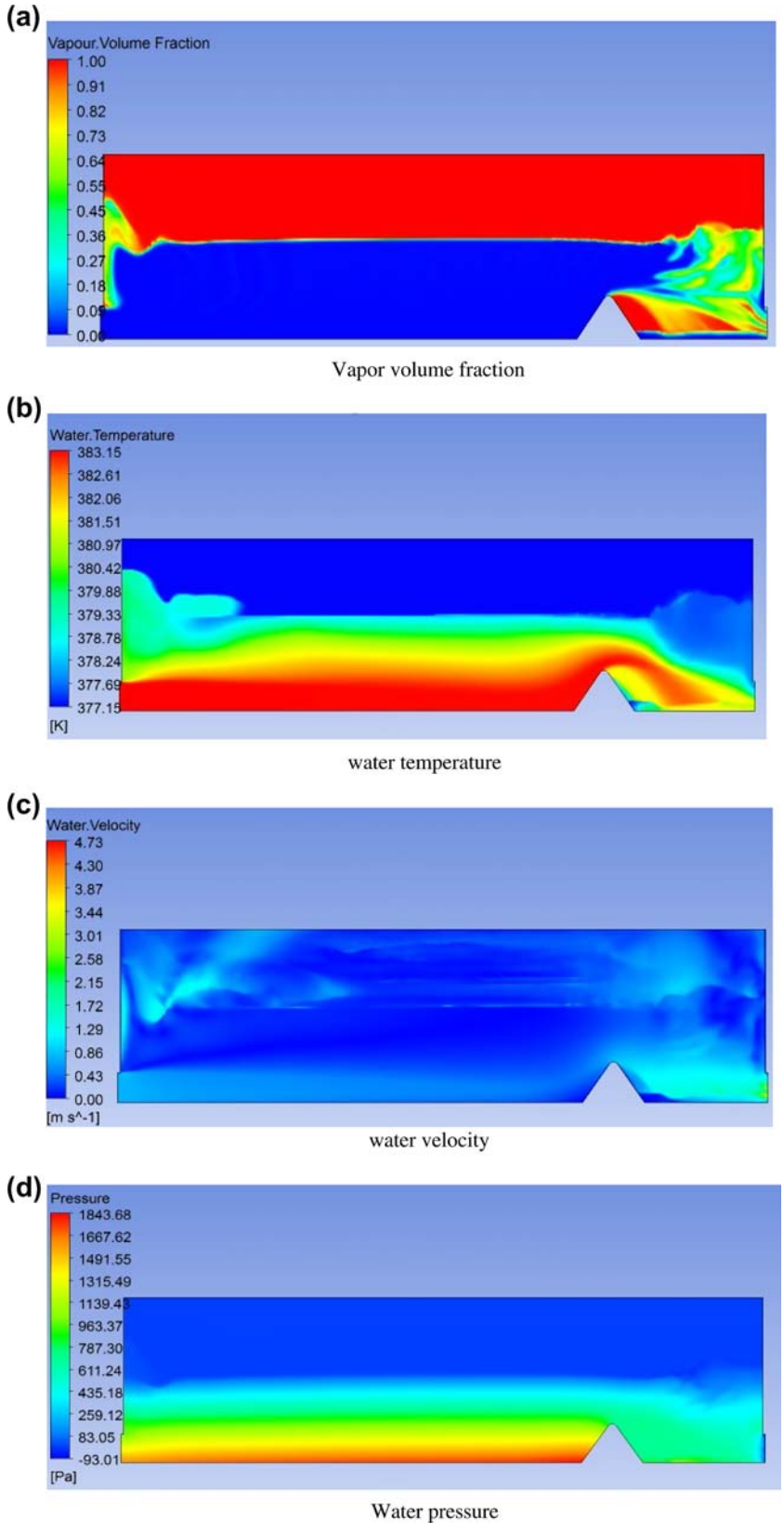


Fig. 10. Thermofluid performance along the FC length (two-third location).

performance in terms of the lowest steam production and the largest steam dryness fraction exiting with the water from the present stage. However, this location is considered the optimal in terms of the hydraulic performance (lowest water pressure drop).

## 4. Conclusion

This article addresses the numerical simulation of the evaporation flashing process and the effect of jumping plate location and number on the thermal and hydraulic performance of MSF FC. A typical in an operating plant, case study has been selected and ANSYS CFX has been implemented to imitate the flashing process characteristics. Those characteristics are represented by the distribution of vapor volume fraction, water temperature, and water velocity along with the FC width. The use of single jumping plate has attained the highest performance compared with the use of two or three plates. The highest performance is identified by a higher steam mass production by 18.2% of flashed vapor rate compared with the reference case of no plates. On the other hand, the use of two jumping plate increases the steam production by the same percentage as the single plate does; however, the calculated pressure drop is higher than that for the single plate by 7.32%. The use of the three jumping plates is considered the worst case in the design; in this case, the steam production has been decreased by 34.3% and an increase in the water pressure drop by 36.3% compared with the reference case. The study also shows that the best location for single plate is the middle in terms of the highest steam production. Alternatively, at one-third location, the flashing process has the lowest volume vapor fraction that could exit with the water to the following stage i.e. the next stage will not be affected by the escaping of flashing vapor that could harm its two-phase flow performance. The main advantage of the two-third location is the minimum pressure drop that can occur in this case but coupled with a higher vapor volume fraction exiting with the water to the next stage. The use of single middle jumping plate assists, therefore, the flashing process to achieve a higher thermal performance in terms of higher steam production by increasing the nucleation sites and flow turbulence.

## Nomenclature

| | | |
|---|---|---|
| $g$ | – | gravitational acceleration, $m/s^2$ |
| $v$ | – | velocity, m/s |
| $\alpha$ | – | phase volume fraction |
| $\rho$ | – | density, $kg/m^3$ |
| $\tau$ | – | stress tensor, Pa |
| $\mu$ | – | dynamic viscosity, Pa.s |
| $P$ | – | pressure, Pa |
| $T$ | – | temperature, ˚C |
| $K$ | – | thermal conductivity, W/m. K |

## Subscripts

| | |
|---|---|
| q | phase (q) |
| p | phase (p) |
| dm | diffusion stress mixture |
| m | mixture |
| tm | turbulent stress mixture |

## Acknowledgment

Computing infrastructure for this research was provided by grants from the Germany Egyptian Research Fund (GERF-STDF), the authors would like to acknowledge their support.

## References

[1] Hassan E.S. Fath, The non-equilibrium factor and the flashing evaporation rate inside the flash chamber of a multi-stage flash desalination plant, Desalination 114(997) (1997) 277–287.
[2] K.W. Seul, S.Y. Lee, Effect of liquid level on flow behaviors inside a multi-stage flash evaporator—a numerical prediction, Desalination 85 (1992) 161–177.
[3] H. El-Dessouky, H. Ettouney, F. Al-Juwlyhel, H. Al-Fulaij, Analysis of multistage flash desalination flashing chambers, Chem. Eng. Res. Des. 82(8) (2004) 967–978.
[4] W.X. Jin, S.C. Low, Investigation of single-phase flow in a model flash evaporation chamber using PIV measurement and numerical simulation, Desalination 150(2002) (2002) 51–63.
[5] D.A. Drew, R.T. Lahey, In Particulate Two-Phase Flow, Butterworth-Heinemann, Boston, MA, 1993.
[6] Hassan E.S. Fath, Mohamed A. Ismail, An online cleaning system to reduce demister fouling in MSF Sidi Krir Desalination Plant, 2 x 5000 $m^3$/day, Desalination 220 (2008) 252–257.
[7] C.W. Hirt, B.D. Nichols, Volume of fluid (VOF) method for the dynamics of free boundaries, J. Comput. Phys. 39 (1981) 201–225.
[8] R.I. Issa, Solution of implicitly discretized fluid flow equations by operator splitting, J. Comput. Phys. 62(1) (1986) 40–65.
[9] S.V. Patankar, Numerical Heat Transfer and Fluid Flow, Hemisphere, Washington, DC, 1980.
[10] T.H. Shih, W. Liou, A. Shabbir, J. Zhu, A new $k$–$\varepsilon$ Eddy-viscosity model for high Reynolds number turbulent flows—model development and validation, Comput. Fluids 24 (1995) 227–238.
[11] D.C. Wilcox, Reassessment of the scale determining equation for advanced turbulence models, J. Am. Inst. Aeronaut. 26 (1988) 1299–1310.
[12] Wilcox, D.C. Turbulence modeling for CFD, third ed., DCW Industries, Inc., La Canada, California, 2006.